Evaluation of Topological Charge Distribution of Structured Soft X-ray Beam

Yuta Ishii*[1] and Yuichi Yamasaki†[1,2,3]

[1]Center for Basic Research on Materials (CBRM), National Institute for Materials Science (NIMS), Tsukuba 305-0047, Japan
[2]RIKEN Center for Emergent Matter Science (CEMS), Wako 351-0198, Japan
[3]International Center for Synchrotron Radiation Innovation Smart, Tohoku University, Sendai 980-8577, Japan

Abstract

Optical structured beams, such as Laguerre-Gaussian and Hermite-Gaussian modes, are characterized by their topological charge, associated with phase rotation and photon orbital angular momentum. Here, we present a quantitative evaluation of highly coherent structured soft X-ray beams generated by diffraction gratings with use of the inline holography technique. The recorded holographic images show good agreement with theoretical calculations based on the scaled fast Fourier transformation. Spatial frequency filtering enables visualization of the phase distribution and reveals the radial distribution of the topological charge intrinsic to the structured beams. This work provides a foundation for quantitatively characterizing structured soft X-ray beams and highlights their potential for probing and manipulating magnetic properties of materials.

Optical Laguerre-Gaussian (LG) beam [**?**], characterized by a helical wavefront, has been the subject of extensive investigation for several decades owing to their rich physical properties, including finite orbital angular momentum (OAM) and topological characteristics arising from azimuthal phase rotation [**?**, **?**, **?**]. An LG beam can be characterized by the topological charge (TC), defined as

$$\ell = \frac{1}{2\pi} \oint_C \nabla\theta(\boldsymbol{\tau}) \cdot d\boldsymbol{\tau}, \tag{1}$$

where $\theta(\boldsymbol{\tau})$ denotes the phase of the photon, and C represents a closed circle encircling the beam's center. The TC corresponds to the number of phase rotations around the beam axis and is directly related to the photon's OAM, expressed as $L = \hbar\ell$. Such structured optical beams have attracted considerable interest due to their potential applications in super-resolution microscopy[**?**], optical tweezers [**?**], and quantum information processing [**?**].

*ISHII.Yuta@nims.go.jp
†YAMASAKI.Yuichi@nims.go.jp

LG beams can be generated through topological distortions, such as dislocation defects in crystalline materials [**?**, **?**]. Moreover, recent studies have explored the interaction between optical vortex beams and magnetic materials, demonstrating their potential for probing and manipulating magnetic properties [**?**, **?**, **?**]. In the soft X-ray regime, previous experimental studies have demonstrated that dislocations in both ferromagnetic and antiferromagnetic lattices can produce LG beams [**?**, **?**, **?**]. Furthermore, soft X-ray LG beams hold considerable promise for characterizing topological dislocations in spin textures by exploiting the topological nature of their phase distribution, as proposed in earlier studies [**?**, **?**]. Soft X-rays are widely employed to investigate magnetic ordering via resonant techniques, such as X-ray magnetic circular dichroism (XMCD) and resonant X-ray scattering (RXS), owing to their sensitivity to spin, orbital, and anisotropic magnetic moments [**?**, **?**, **?**]. Therefore, the visualization of the phase structure of LG beams and the quantitative evaluation of their TCs are essential for the application of soft X-ray LG beams to a broad range of magnetic materials. Especially, the TC distribution in LG beams scattered from materials reflects the spatial distribution of topological dislocations in magnetic materials. Thus, determining the spatial distribution of the TC is crucial not only for visualizing and evaluating dislocations in magnetic textures, but also for investigating the interaction between LG beams and magnetic materials through the OAM carried by the beams.

For the quantitative evaluation of TC, we have recently developed an inline holography technique based on coherent soft x-ray microscopy [**?**, **?**]. In this method, an interference pattern formed by the reference beam and the waves diffracted from the sample is detected using a two-dimensional detector. The phase distribution of the diffracted wave is encoded within the interference pattern and can be retrieved through Fourier analysis. In our previous work, we successfully visualized the rotational phase distribution of an LG soft X-ray beam generated by a fork grating using this technique. However, the holographic patterns lack sufficient precision for a quantitative evaluation of TC due to the limited coherence of the incident X-rays. Consequently, quantitative analyzes, such as determining the spatial distribution of the photons' TCs, remain challenging.

Here, we report inline holography measurements of highly coherent LG and Hermite-Gaussian modes (HG) soft X-ray beams generated using two types of diffraction gratings. Inline holography measurements with highly coherent incident soft X-rays, as available at the synchrotron facility NanoTerasu in Japan, enable the quantitative visualization of their phase distributions and the determination of the radial distribution of TC. This approach provides a direct and quantitative characterization of the phase structure inherent in structured soft X-ray beams.

Inline holography measurements were performed at BL14U, NanoTerasu, using the soft X-ray microscope [**?**]. The experimental setup is depicted in Fig. 1(a). The incident X-ray beam was focused using a Fresnel zone plate (FZP) with outer and center beam-stopper radii of 60 and 30 μm, respectively, and the number of zones $N = 231$. The wavelength of the X-ray is tuned to $\lambda = 1.6$ nm, which ideally results in a focal length of 1.5 mm via an FZP. The higher order diffraction waves from the FZP were sorted by an order sorting aperture (OSA) with a diameter of 20 μm. The gratings with a circular outline for generating structured soft X-rays were placed 900 μm downstream from the first focal point of the FZP. The pitch and the radius of the gratings are 200 nm and 2.5 μm, respectively. The diffracted X-ray wave from the grating interferes with the transmitted direct X-ray beam through the surroundings of the grating. The interference patterns are recorded using a Charge Coupled Device (CCD) camera, which is positioned 0.345 m away from the sample.

Here, two types of gratings are used to generate two types of structured soft X-ray beams: LG

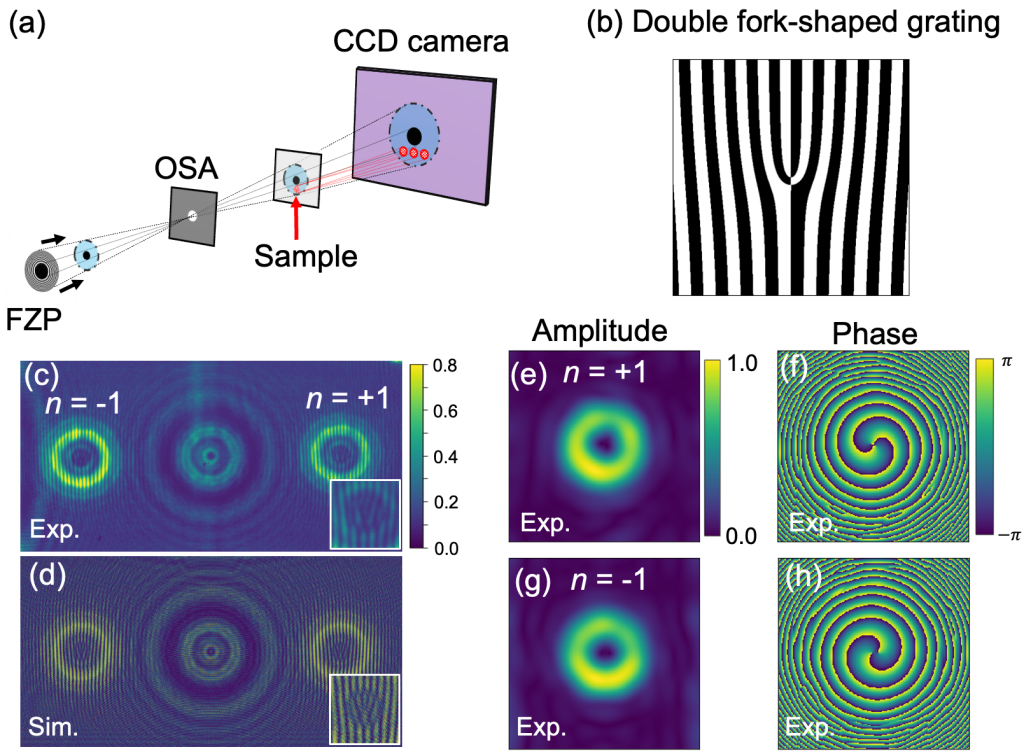

Figure 1: (Color online) (a) Experimental setup of the inline holography based on soft x-ray microscopy equipment. (b) Schematic view of double fork-shaped grating with topological number $b = 2$. The black and white regions represent the amplitude of the grating' s transmittance. (c) Holographic image of the $n = \pm 1$ diffraction waves from the fork grating with $b = 2$. Inset shows the enlarged view of the $n = +1$ diffraction waves. (d) Simulation results obtained by scaled fast Fourier transformation (FFT) calculation. (e)-(g) Experimentally obtained amplitude and phase distributions of the $n = \pm 1$ soft x-ray diffraction waves.

and HG modes. These gratings were made from Ta metal with a thickness of 300 nm deposited onto a membrane of Si_3N_4, and were fabricated by NTT-AT, Japan. Incident X-rays can transmit around the gratings, which interferes with the diffracted soft x-rays from the grating.

Figure 1(c) presents the holographic image of the first-order diffracted soft x-ray waves ($n = \pm 1$) from a double-fork-shaped grating characterized by a topological number $b = 2$, whose schematic view of the grating is shown in Fig. 1 (b). The transmittance of the fork grating is expressed as [**?**]

$$t(\rho, \phi) = \frac{1}{2}\left(1 + \mathrm{sgn}\left[\sin\left(\frac{2\pi}{d}\rho\cos\phi + b\phi\right)\right]\right), \tag{2}$$

with two-dimensional polar coordinates (ρ, ϕ), where d is the pitch of the grating far from the center. The vortex beam with OAM $\ell = nb$ is generated as the n-th Bragg diffraction from the grating. Distinct stripe patterns superimposed on a reference beam pattern are observed in both diffracted waves, accompanied by double fork-shaped structures near the center, as shown in the inset of Fig. 1(c). These features signify interference between LG beams with $\ell = \pm 2$ and the reference beam transmitted around the grating. The results of a numerical simulation based on

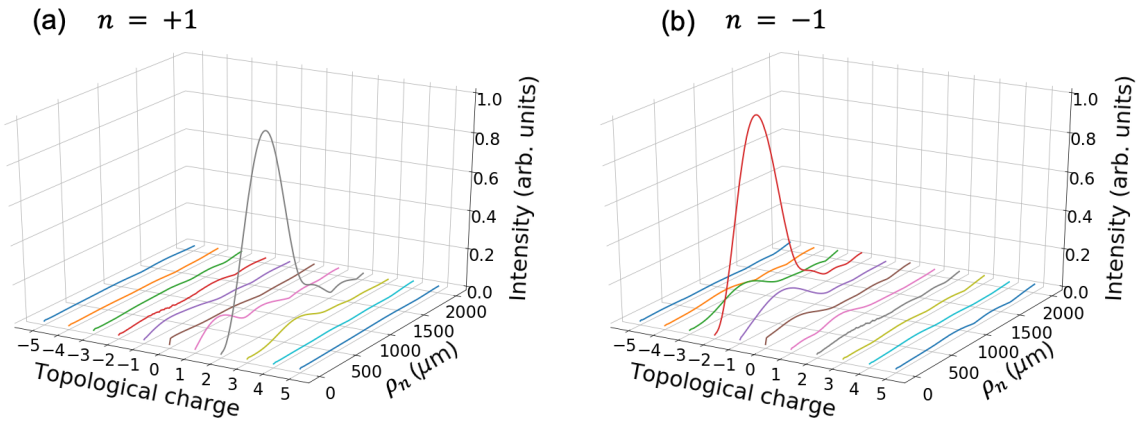

Figure 2: (Color online) Distributions of topological charge of the diffraction waves (a) $n = 1$ and (b) $n = -1$ along the radial direction ρ_n.

a scaled fast Fourier transform (FFT) [**?**] are shown in Fig. 1(d). The experimentally obtained holographic image exhibits excellent agreement with the simulated pattern. It is noted that the weaker intensity of the $n = 0$ diffraction wave compared with the $n = \pm 1$ diffraction waves can be reproduced by including the imaginary part of the complex refractive index of the Ta-based FZP, which can reduce the intensity through interference with the direct beam.

The interference intensity of the n-th Bragg diffraction generated by a fork grating with the topological number b is expressed as [**?**, **?**]

$$I_{nb}^{\text{inter}} \propto \mathscr{J}'_{nb}(\rho_n) \sin\left[kR_2 + nb\phi_n + \alpha_{nb} + n(b-1)\frac{\pi}{2}\right], \tag{3}$$

where (ρ_n,ϕ_n) denote the local cylindrical coordinates defined with respect to the center of the n-th Bragg wave, and k represents the photon wavenumber. The parameter R_2 characterizes the phase difference between the reference wave and the diffracted wave. The function $\mathscr{J}'_{nb}(\rho_n)$ is given as

$$\mathscr{J}'_{nb}(\rho_n) = \int_0^a e^{if_0\rho^2} \rho J_{nb}(\rho_n\rho) d\rho = |\mathscr{J}'_{nb}(\rho_n)| e^{i\alpha_{nb}}, \tag{4}$$

with the nb-th Bessel function of the first kind J_{nb}. Consequently, both the amplitude and phase information of the scattered wave are encoded within the interference intensity pattern and can be retrieved through Fourier-transform analysis. The amplitude $A_n(r,\phi)$ and phase $\theta_n(r,\phi)$ distributions of the $n = \pm 1$ diffracted waves, $f_n(r,\phi) = A_n(r,\phi)\exp[i\theta_n(r,\phi)]$, are reconstructed using frequency-space filtering, as shown in Figs. 1 (e)-(h). Detailed descriptions of the analysis procedure are provided in our previous reports [**?**, **?**]. Experimentally, the reconstructed amplitude and phase exhibit annular and double-spiral phase structures, respectively. Furthermore, the rotational direction of the spiral phase is inverted between the $n = \pm 1$ waves, demonstrating characteristics of the LG beam with $\ell = \pm 2$.

The high coherence of the incident soft X-rays, together with the precise interference patterns, enables the quantitative analysis of the scattered structured soft X-rays, including the determination of the photon TC distribution along the radial direction ρ_n. The diffracted waves are decomposed

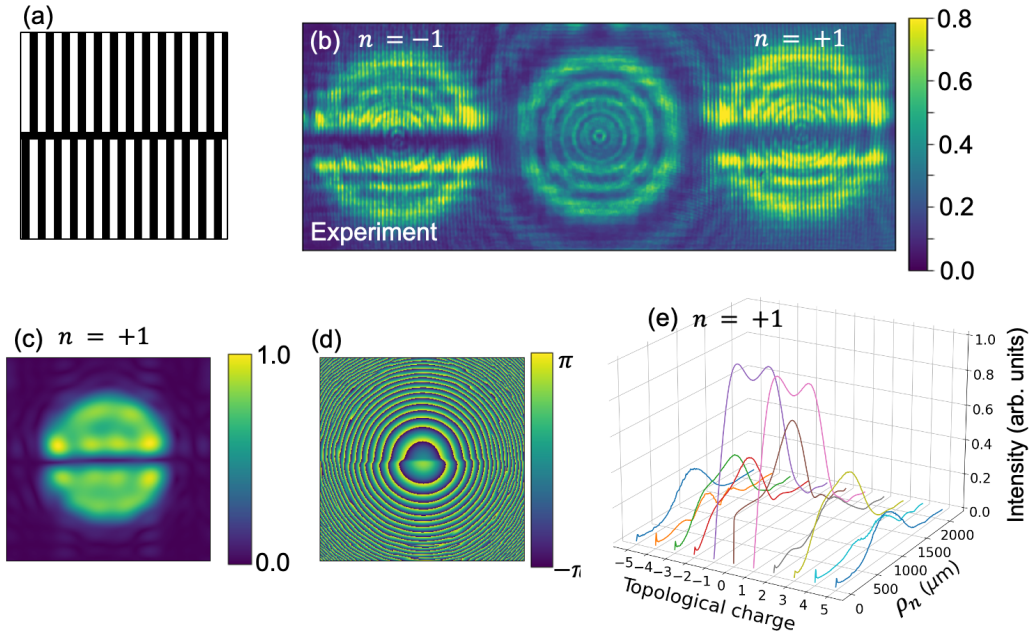

Figure 3: (Color online) (a) Schematic of grating producing $HG_{0,1}$ mode waves as $n = \pm 1$ diffraction. (b) Holographic image of direct beam and $n = \pm 1$ diffracted waves. Experimentally obtained (c) amplitude and (d) phase distribution of $n = 1$ HG waves. (e) Radial distributions of TC for $n = 1$ HG wave.

into the components with ℓ using the following equation;

$$L_n^{\ell}(\rho_n) = \int_0^{2\pi} f_n^{\exp}(\rho_n, \phi_n) \exp(-i\ell\phi_n) d\phi_n. \tag{5}$$

with experimentally obtained wave $f_n^{\exp}(\rho_n, \phi_n)$. This equation provides the radial distribution of each TC component. Figures 2(a) and (b) show the radial TC distributions $L_n^{\ell}(\rho_n)$, for the $n = \pm 1$ diffracted waves. Pronounced peaks are observed at $\ell = \pm 2$ and around $\rho_n \sim 500$ μm for the $n = \pm 1$ waves, respectively, while contributions from other components are negligible. These results demonstrate that the rotational phase structure and the TC distribution of the LG soft X-ray beams are quantitatively determined with high fidelity.

While the above results demonstrate the applicability of the present technique to LG modes with helical phase structures, it is also important to verify its capability for beams with fundamentally different symmetries. In this context, we extend the analysis to the HG modes, which are characterized by Cartesian symmetry and lack orbital angular momentum [**?**]. The transmittance of the grating employed in this study is schematically illustrated in Fig. 3 (a), where the phase of the grating is shifted by π between its upper and lower regions. Such grating generates an $HG_{0,1}$ mode beam, in which the photon phase features a π shift between the upper and lower regions relative to the beam center. The holographic image obtained through inline holography measurements is presented in Fig. 3 (b).

Diffracted wave patterns accompanied by interference fringes are clearly observed for the $n = \pm 1$ diffraction waves. For both waves, the stripe patterns in the upper half of the diffraction pattern are out of phase by π with respect to those in the lower half. The amplitude $A_n(r, \phi)$ and phase

$\theta_n(r, \phi)$ distributions for the $n = 1$ diffraction wave are extracted as shown in Figs. 3(c) and (d), respectively. These results confirm that phase inversion occurs along the horizontal central axis for the $HG_{0,1}$ mode.

Applying the same analysis method as described in Eq. **??**, Fig. 3 (e) presents the TC distribution of the $n = 1$ diffracted wave. Pronounced TC components are observed at $\ell = \pm 1$. An HG-mode beam can be expressed as a superposition of two LG modes; specifically, the $HG_{0,1}$ mode corresponds to LG modes with $\ell = \pm 1$. These results demonstrate that the present technique enables the quantitative determination of the TC components intrinsic to HG-mode beams. In addition, minor contributions from several other TC components are also detected. These are likely attributed to limitations in the fabrication accuracy of the grating or to residual contamination from the $n = 0$ diffraction beam. This observation further suggests that the present technique is sufficiently sensitive to resolve TC components even in soft X-ray waves generated from imperfect or arbitrary defect structures.

In this study, we have demonstrated the quantitative evaluation of structured soft X-ray beams, specifically LG and HG mode waves. By employing highly coherent soft X-rays, the interference patterns obtained through inline holography measurements exhibit excellent agreement with theoretical simulations. Further analysis allows for the quantitative determination of the TC distributions intrinsic to the structured beams. These results pave the way for the development of structured soft X-ray beams for probing and manipulating magnetic materials.

Acknowledgments

We thank Tetsuya Nakamura, Yoshinori Kotani, Akiho Sumiyoshiya, Yusuke Tanimoto, and Taishi Kawabata at PhoSIC for supporting us with the CDI experiments at NanoTerasu BL14U, and Taka-hisa Arima and Yusuke Wakabayashi for fruitful discussions. This work was partially supported by JSPS KAKENHI (Project Nos. JP19K23590, JP19H04399, JP20K20107, JP23K17145, JP24K03205, JP24H01685, JP24K17603, JP25K03387), by PRESTO (JPMJPR2102) and CREST (JPMJCR1861 and JPMJCR2435) Japan Science and Technology Agency (JST). This work was supported by MEXT Quantum Leap Flagship Program (MEXT Q-LEAP) Grant Number JPMXS0118068681. The synchrotron X-ray inline holography experiments were performed at the NanoTerasu BL14U-soft X-ray beamline of the Photon Science Innovation Center (PhoSIC) under the Coalition Program.

References

[1] M. W. Beijersbergen, L. Allen, H. E. L. O. van der Veen, and J. Woerdman: Opt. Commun. **96** (1993) 123.

[2] L. Allen, M. Beijersbergen, R. J. C. Spreeuw, and J. Woerdman: Phys. Rev. A **45** (1992) 8185.

[3] Y. Shen, X.Wang, Z. Xie, C.Min, X. Fu, Q. Liu, M. Gong, and X. Yuan: Light-Sci. Appl. **8** (2019) 1.

[4] M. Cheng, W. Jiang, L. Guo, J. Li, and A. Forbes: Light-Sci. Appl. **14** (2025) 4.

[5] X. Qiu, F. Li, W. Zhang, Z. Zhu, and L. Chen: Optica **5** (2018) 208.

[6] D. G. Grier: Nature **424** (2003) 810.

[7] G. Molina-Terriza, J. P. Torres, and L. Torner: Nat. Phys. **3** (2007) 305.

[8] J. C. T. Lee, S. J. Alexander, S. D. Kevan, S. Roy, and B. J. McMorran: Nat. Photonics **13** (2019) 205.

[9] N. Khan, R. Jangid, T. Stanislavchuk, A. Stein, O. Chubar, A. Barbour, A. Sirenko, V. Kiryukhin, and C. Mazzoli: Opt. Lett. **51** (2026) 877.

[10] H. Fujita and M. Sato: Phys. Rev. B **95** (2017) 054421.

[11] M. A. Yavorsky, E. V. Barshak, V. N. Berzhansky, S. D. Lyashko, M. A. Kozhaev, A. Y. F. D. V. Vikulin, and V. I. Belotelov: Phys. Rev. Appl. **18** (2022) 054008.

[12] S. H. Guan, Y. Liu, Z. P. Hou, D. Y. Chen, Z. Fan, M. Zeng, X. B. Lu, X. S. Gao, M. H. Qin, and J.-M. Liu: Phys. Rev. B **107** (2023) 214429.

[13] J. S. Woods, X. M. Chen, R. V. Chopdekar, B. Farmer, C. Mazzoli, R. Koch, A. S. Tremsin, W. Hu, A. Scholl, S. Kevan, S. Wilkins, W.-K. Kwok, L. E. De Long, S. Roy, and J. T. Hastings: Phys. Rev. Lett. **126** (2021) 117201.

[14] M. Fanciulli, M. Pancaldi, E. Pedersoli, M. Vimal, D. Bresteau, M. Luttmann, D. De Angelis, P. c. v. R. Ribič, B. Rösner, C. David, C. Spezzani, M. Manfredda, R. Sousa, I.-L. Prejbeanu, L. Vila, B. Dieny, G. De Ninno, F. Capotondi, M. Sacchi, and T. Ruchon: Phys. Rev. Lett. **128** (2022) 077401.

[15] M. R. McCarter, A. I. U. Saleheen, A. Singh, R. Tumbleson, J. S. Woods, A. S. Tremsin, A. Scholl, L. E. De Long, J. T. Hastings, S. A. Morley, and S. Roy: Phys. Rev. B **107** (2023) L060407.

[16] Y. Ishii, K. Yamamoto, Y. Yokoyama, M. Mizumaki, H. Nakao, T.-h. Arima, and Y. Yamasaki: Phys. Rev. Appl. **14** (2020) 064069.

[17] Y. Ishii, H. Nakao, M. Mizumaki, Y. Wakabayashi, T. h. Arima, and Y. Yamasaki: Sci. Rep. **12** (2022) 1044.

[18] B. T. Thole, P. Carra, F. Sette, and G. van der Laan: Phys. Rev. Lett. **68** (1992) 1943.

[19] P. Carra, B. T. Thole, M. Altarelli, and X. Wang: Phys. Rev. Lett. **70** (1993) 694.

[20] Y. Yamasaki, Y. Ishii, and N. Sasabe: Sci. Technol. Adv. Mater. **26** (2025) 2513217.

[21] Y. Ishii, Y. Kozuka, S. Kawachi, T. Ito, Y. Wakabayashi, H. Nakao, T.-H. Arima, and Y. Yamasaki: Sci. Technol. Adv. Mater. Methods **5** (2025) 2586300.

[22] D. H. Bailey and P. N. Swarztrauber: SIAM Rev. **33** (1991) 389.